Fast Hotspot Detection in SFCLs by Exploiting Strain Response in Optical Fiber Sensing

A. Akbar, N. Riva, Z. Yang, Luc Thévenaz, and B. Dutoit

***Abstract*—Superconducting fault current limiters (SFCLs) can be used to limit fault currents in both meshed DC and AC grids by transitioning from superconducting to resistive state, in the presence of high currents. While the device is theoretically a great way to protect grids, the inherent inhomogeneity of critical current along the superconductor length can lead to localized heating, called hotspots, and ultimately destruction of the SFCL device. At EPFL under the European Union project Fastgrid, an extremely efficient Mach-Zehnder interferometer (MZI) based optical fiber sensing technique has been developed and patented that can detect even singular hotspots within 15 ms to protect SFCLs. The MZI response is characterized by a strain sensitive as well as a temperature sensitive contribution. This paper outlines an investigation by means of FEM modeling into the response sensitivity. A 2-D thermal model of the superconducting tape and optical fiber was made to study thermal transfer to the optical fiber from the REBCO tape. The simulation results showed that temperature rise observed in the optical fiber is slower than the MZI response time, proving a strain sensitive response in the experiment measurements. Sound mechanical coupling between the optical fiber and the superconductor tape can enhance strain transfer to the optical fiber and hence reduce hotspot detection time. With this improved performance, the health monitoring for SFCLs can be much more efficient and reliable.**

***Index Terms*—HTS, SFCL, hotpot detection, quench detection, optical fiber sensing, Mach-Zehnder interferometer.**

I. Introduction

RENEWABLE energy generation is an increasing trend in these times. With the Sustainable Development Goals, it has been projected that the share of renewable energy generation will increase to 63% in the primary energy supply, and to 85% in the power sector by 2050 [1]. Consequently, High Voltage Direct Current (HVDC) transmission will become increasingly relevant. HVDC is desirable because of its numerous advantages over AC transmission, like higher power transfer capabilities and lower line losses over longer distances [2]. At present, HVDC links connect offshore renewable energy generation to the distribution grid; however, with increased renewable energy contribution, the grid will gradually evolve into a meshed HVDC grid. Meshed HVDC grids come with the unresolved issue of fault handling; these grids are susceptible to high fault currents which need to be detected and cleared within the order of 10 ms [3]. The protection mechanisms that are used for AC grids will not be suited to address the protection of a low inertia meshed HVDC grid [4]. SFCLs are good candidates which are capable of protecting meshed HVDC grids with their quick transition from superconducting state to resistive state in the presence of high currents [5]. However, SFCLs need to be protected against hotspots which arise because of the inhomogeneous critical current along the length of the superconductor. The superconductor critical current normally lies in a band, ranging from minimum critical current value ($I_{\mathrm{c,min}}$) to the maximum critical current value ($I_{\mathrm{c,max}}$). This inhomogeneity can lead to non-uniform transitions of the superconductor to resistive state. Hence, in the case of an operating current that lies between $I_{\mathrm{c,min}}$ and $I_{\mathrm{c,max}}$, singular or a few localized hotspots may arise in the SFCL; if these hotspots go undetected there is a risk of thermal runaways and localized destruction of the SFCL device. In order to prevent such an event from happening, a hotspot detection mechanism is required that is capable of detecting hotspots within 15 ms for reliable SFCL health monitoring.

Optical fiber sensing is an attractive solution to detect hotspots in SFCLs because optical fibers are capable of working in high voltage environments and offer numerous advantages of being inexpensive, light-weight, not influenced by the magnetic field, and chemically inert. Distributed optical fiber sensing using Rayleigh Backscattering has been proposed and patented for hotspot detection in high temperature superconductors [6]. This technique is capable of providing location of the hotspot within the superconductor, but remains slow and expensive for SFCL protection. Meanwhile, other quasi-distributed optical fiber sensing techniques like Fiber Braggs Grating come with the disadvantage of information loss between the sensing locations [7]. For applications like SFCL, a cost-effective MZI based optical fiber sensing technique for extremely fast detection of hotspots within 15 ms has been developed and patented by EPFL under the EU FastGrid project (the reference for the patent will soon be discoverable) [8], [9]. Although the information about the hotspot location is not provided by this technique, it is sufficient to trigger a rapid alert for hotspot occurrence and subsequent device protection mechanisms for SFCL protection. The previous manuscript addressed how the response time varied

Manuscript received November 30, 2020; revised February 11, 2021 and February 17, 2021; accepted February 17, 2021. Date of publication February 23, 2021; date of current version April 22, 2021. This work was supported by the European Union's Horizon 2020 Research and Innovation Program under Grant 721019. *(Corresponding author: A. Akbar.)*

A. Akbar, N. Riva, and B. Dutoit are with the SCI-IC-BD, École Polytechnique Fédérale de Lausanne, CH-1015 Lausanne, Switzerland (e-mail: arooj.akbar@epfl.ch; nicolo.riva@epfl.ch; bertrand.dutoit@epfl.ch).

Z. Yang and Luc Thévenaz are with the SCI-STI-LT, École Polytechnique Fédérale de Lausanne, CH-1015 Lausanne, Switzerland (e-mail: zhisheng.yang@epfl.ch; luc.thevenaz@epfl.ch).

Color versions of one or more figures in this article are available at https://doi.org/10.1109/TASC.2021.3061346.

Digital Object Identifier 10.1109/TASC.2021.3061346

with the quality of optical fiber integration; thereby deducing, that the quality of integration impacts strain transfer to the optical fiber, which required a more investigative study [10]. In this paper, we present a simple 2- D FEM thermal model and experimental results using two integration mediums varying in terms of thermal conductivity, to quantitatively assess if the fast response of the MZI technique occurred due to strain or temperature change experienced by the optical fiber.

II. Mach-Zehnder Method

The MZI works on the interference principle and requires two optical fibers. One optical fiber acts as a reference while the other is coupled with the superconductor, as shown in Fig. 1(a). A polarization controller is present on the reference arm and under optimum conditions, the light polarizations in both branches are well aligned at the coupler. Light is split into the two optical fibers at the input and recombined at the output where interference occurs.

The MZI output at the photo- detector (i.e., the interference pattern) can be expressed as :

$$Interference\ Pattern \propto \left[1 + \cos\left(\phi_{12} - \pi + \Delta\phi_{\mathrm{H}}\right)\right], \quad (1)$$

$$\Delta\phi_{\mathrm{H}} \propto \left(\left\{1 - \rho_a\right\}\Delta\varepsilon + \left[\alpha_O + \xi\right]\Delta T\right) \quad (2)$$

Where ϕ_{12} is the initial phase shift between the two light paths and $\Delta\phi_{\mathrm{H}}$ is the phase shift due to hotspot and ambient factors; $\Delta\phi_{\mathrm{H}}$ depends on the change in strain ($\Delta\varepsilon$) and temperature change (ΔT) as expressed in (2) [11], where ρ_a, α_O and ξ, are the photo- elastic coefficient, thermal expansion coefficient, and thermo-optic coefficient of the optical fiber respectively. (2) comprises a strain dependent and a temperature dependent term. Together, the two terms define the MZI response sensitivity.

In the absence of a hotspot, both $\Delta\varepsilon$ and ΔT arise due to environmental perturbations (like temperature, acoustic noise, and vibrations), which results in a slow variation of $\Delta\phi_{\mathrm{H}}$. The interference pattern in this case, therefore, exhibits slow fluctuations without a discernable pattern. When there is a hotspot in the superconductor, the consequent temperature rise causes an increment of ΔT with positive sign in the optical fiber, meanwhile $\Delta\varepsilon$ also increments because of the strain imposed on the optical fiber due to the thermal expansion of the conductor materials, mainly Hastelloy. Subsequently, as the two terms in (2) increase, $\Delta\phi_{\mathrm{H}}$ continuously increments from 0 to 2π, within few ms, in response to the hotspot. As $\Delta\phi_{\mathrm{H}}$ changes, the MZI output displays rapid, continuous periodic amplitude variations between 0 and 1 (normalized), with a frequency dependent upon the rate of temperature change; this signals the presence of (at least) a single hotspot.

From (2), it can be deduced that the manner in which the optical fiber is integrated with the superconductor plays a crucial role in determining the response time. Since the optical fiber shows sensitivity to both strain and temperature it is inferred that it is important to create a strong mechanical coupling between the optical fiber and the superconductor. This can guarantee a large strain sensitivity which leads to a quick response to a hotspot, because the change in strain is felt earlier than thermal transfer, by the optical fiber. This dependence of response quality on the coupling that exists between the optical fiber and the conductor is summarized in Table I and investigated in this paper.

TABLE I
Dependence of MZI Response on Optical Fiber Integration

Coupling	Response type	Response speed
Thermal	Temperature sensitive	Slow
Mechanical	Strain sensitive	Fast
Thermal & Mechanical	Strain dominated	Fast

Table summarizing how the MZI response depends on the type of coupling that exists between the optical fiber and the superconducting tape.

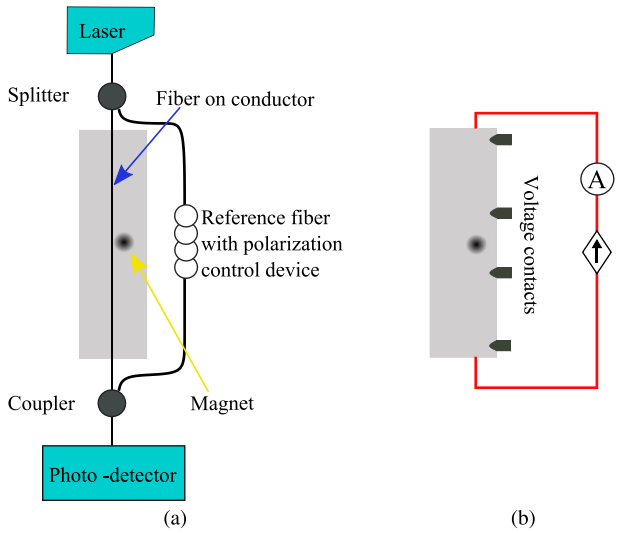

Fig. 1. (a) Optical setup: The MZI configuration with two optical fibers, one integrated on the surface of the superconductor and the second one acting as reference, there is a magnet placed on the superconductor to create a weak point. (b) Electrical setup: The experiment setup comprising the electrical circuit, and voltage contacts placed around the magnet and the full sample length.

III. Experimental Procedure

The optical fiber was integrated along 1 m length of a 4 mm wide copper stabilized superconducting tape manufactured by SuperPower (SCS4050-AP). The critical current of the sample was 125 A (at 77 K and self-field conditions), provided by the manufacturer. Two different integration methods were used: one in which the optical fiber was glued to the superconductor by means of Stycast (Stycast was used to enhance thermal transfer to the optical fiber) and the second one where the optical fiber was taped using Kapton (which has a lower thermal conductivity than Stycast). The thermal conductivity of Stycast is 0.9 $\mathrm{W/(m \cdot K)}$ at 77 K and that of Kapton is 0.12 $\mathrm{W/(m \cdot K)}$ [12], [13]. A 10 mm diameter magnet was placed in the center of the sample to create a weak point of a known location, as shown in Fig. 1. The sample was immersed in liquid nitrogen bath at

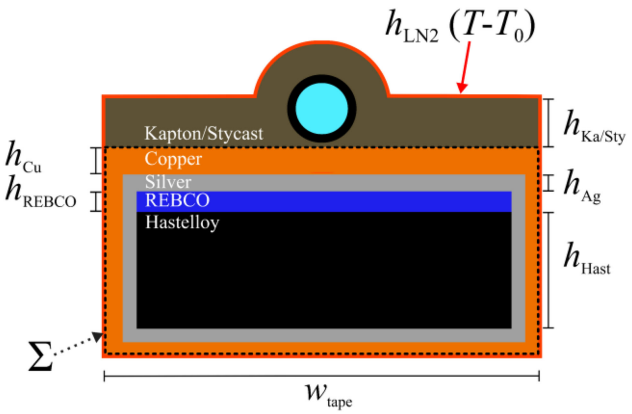

Fig. 2. Schematic representation (not in scale) of the 2-D thermal model showing the cross-section of the superconductor tape and the boundary condition applied to account for convective heat transfer in liquid nitrogen bath. The quantity Σ indicates the surface on which the heat source was applied.

77 K, and a current pulse was injected through the sample using a DC current pulser. Voltage around the weak point (10 mm length) as well as along the sample length (1m) was measured. The MZI output was also acquired. These experiment measurements are plotted along with the simulation results, in Section V.

IV. Simulation: 2-D Thermal Model

In this manuscript we use simulation results to characterize the technique response for two integration media (Kapton and Stycast) with different thermal conductivities. As mentioned in our previous manuscript, a sensitivity analysis was important because of how the technique response varied with the variation in integration quality between the optical fiber and the superconductor. Here, we demonstrate that the thermal transfer is much slower than the response of the optical fiber observed in the experiments. Since our purpose is to evaluate the thermal transfer from a hotspot in the conductor to the optical fiber, an electrothermal model was not necessary at this stage. Instead, we used a 2-D thermal model simulating the cross section of the tape (Fig. 2). We assumed that the thermal and geometrical properties of the conductor do not vary significantly along the length. The heat generated during a current pulse originated from the joule losses $Q = E \cdot J$, where E is the electric field applied on the tape, and J is the current density. If we consider all the conductive parts of the tape as a homogeneous heat source, we can write:

$$Q = E \cdot J = \frac{V \cdot I}{\Omega}, \tag{3}$$

where V is the voltage measured over a given section of the tape l, I is the measured current and Ω is the volume of the conductor (with copper stabilizer with a thickness of 10 μm, 1 μm REBCO,1 μm silver, and 50 μm Hastelloy).

The Kapton/Stycast, being insulators, did not contribute to the joule heating since no current can possibly flow in them, and thus they are not considered in the heat-source equation. The model was developed in COMSOL Multiphysics using the Heat Transfer Module (ht) [12]. The temperature dependence of all the material properties was taken into account. The material properties utilized in the model can be found in [13],[16]. The heat equation is solved on a 2-D domain (Fig. 2) and can be written as (4), where on the left side of (4), we have the mass density $\rho_{\text{mass}}(T)$, the specific heat capacity $C_{\text{p}}(T)$ and the thermal conductivity k. On the right side of (4), we have the heat source term and a cooling term. The heat source is $V \cdot I/\Omega$, and was obtained using the experimental measurements (V and I) and applied on the conductor volume $\Omega = l \cdot \Sigma$, where Σ is the cross section of the tape (dashed line enclosing box in Fig. 2).

$$\rho_{\text{mass}}(T)\, C_{\text{p}}(T)\, \frac{\partial T}{\partial t} - \nabla \cdot (k \nabla T) = \frac{V \cdot I}{\Omega} - h_{\text{LN2}} \cdot (T - T_0), \tag{4}$$

The heat exchange with the liquid nitrogen was considered by applying a boundary condition, as indicated in Fig. 2. The heat transfer coefficient $h_{\text{LN2}}(T - T_0)$ is a function of the difference of temperature, ΔT [17], but for a better readability it is written as h_{LN2}.

V. Results and Discussion

The results for both Kapton and Stycast are plotted in Fig. 3(a) and (b) respectively. The graphs show the experiment results as well as the simulated evolution of temperature with time in the REBCO (dashed black) and optical fiber (continuous black) domains. The temperature profiles in time were calculated for the REBCO and the optical fiber core, by taking an average over the respective volumes. For the experiment results the graphs show the injected current in the sample (in red), the two voltages measured on the sample length (dotted blue), as well as around the magnet (continuous blue). The initial peak in the sample voltage for the case in Fig. 3(a) arises due to circuit inductance. In both cases in Fig. 3(a) and (b), it can be seen that the maximum voltage reached in the sample is similar to the maximum voltage in the hotspot; this signifies a single point heating (in the region of the magnet) in the superconductor sample. The MZI output is plotted in green and is the non-normalized voltage output from the photo- detector, plotted with a shift along the y-axis for easy viewing of the plots. It can be seen that the MZI output shows no observable pattern before the event of the hotspot (voltage rise in the sample), and as the voltage in the sample rises, the MZI output switches to rapid amplitude variations, signaling a hotspot. The frequency of this amplitude variation is proportional to the rate of temperature change as explained in Section II. Given that, it is necessary to explain here that the frequency of oscillations in Fig. 3(a) is lower than the frequency of the oscillations in Fig. 3(b) because of the lower power dissipated, hence smaller temperature change, in the sample for the case in Fig. 3(a). The MZI response for both cases, Fig. 3(a) and (b), however, is quick and within 15 ms, as shown in the zoomed in graphs in Fig. 3. In order to understand the fast MZI response, it is interesting to look at the temperature curves obtained from our 2-D thermal model in Fig. 3. These simulation results show that the temperature change in the optical fiber, for both the cases shown in Fig. 3, is negligible (almost zero) during

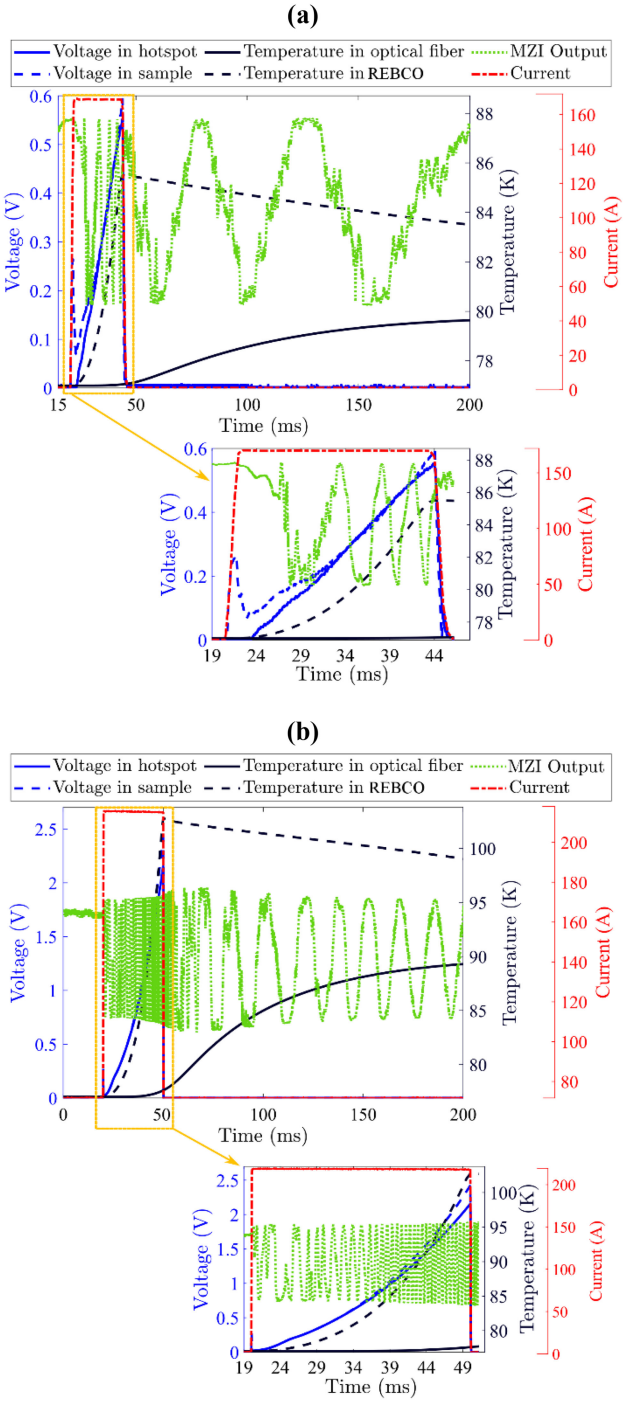

Fig. 3. Simulation results for temperature in REBCO and optical fiber (in black) for optical fiber integrated with Kapton (a) and Stycast (b) plotted along with the experimental measurements and showing the observed MZI response before the temperature peaks in the optical fiber.

the event of the hotspot and peaks much later. However, the MZI response is observed even in the absence of a temperature change experienced by the optical fiber. With this result, it can be deduced that the instantaneous MZI response arises because of the strain sensitive term in (2) and the optical fiber, therefore, experiences the change in strain earlier than the temperature

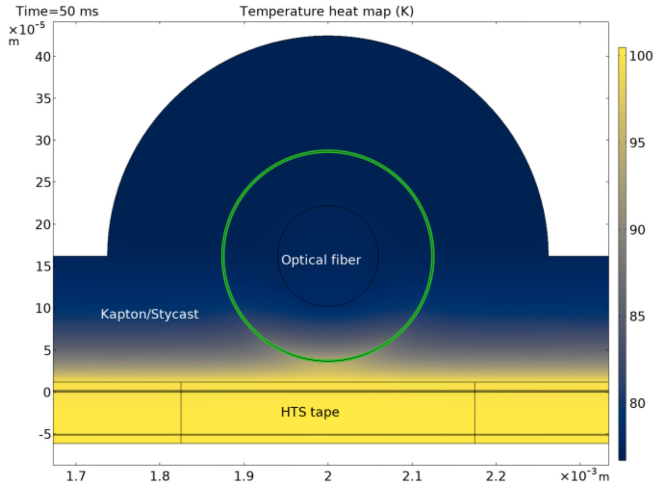

Fig. 4. Heatmap obtained from the thermal model shows the temperature gradient along the cross-section.

change. Another interesting result to note is that, even though Stycast presents a higher thermal conductivity than Kapton, the temperature change in the optical fiber is still not fast enough to influence the MZI response within 15 ms. In this manuscript therefore, we eliminate the dependence of the instantaneous response of our technique on thermal transfer.

The temperature change in the optical fiber is also impacted by the heat exchange with liquid nitrogen. Fig. 4 shows the heatmap obtained for the thermal model at the end of the current pulse (around 50 ms). Since the heat source was applied only on the conductor (volume Ω), the heat flux moves towards the upper part of the tape, generating a temperature gradient visible in Fig. 4: the temperature ranges from 100 K in the bottom part of the tape down to 80 K in the upper part of the tape. The time-delay observed between the temperature curves for REBCO and the optical fiber is explained by both heat conduction across the tape and the cooling properties of the liquid nitrogen.

VI. Conclusion

The optical fiber sensing technique developed at EPFL for hotspot detection in SFCLs enables extremely fast hotspot detection using an economically feasible setup. Proper optical fiber integration technique is necessary for rigidity, to ensure optimal strain transfer to the optical fiber. The 2-D FEM thermal model developed validates this deduction by showing that the MZI response to a hotspot occurs almost instantaneously and before a temperature change is experienced by the optical fiber. It is the strain transfer which leads to an instantaneous response to a hotspot. Future work on this technique is extending the experiments to long sample lengths and the FastGrid pancake to further study the technique feasibility. This ground-breaking technique, can enable a wide scale use of not only SFCLs but also other HTS applications by providing a reliable and efficient health monitoring system to ensure resilience against hotspots.

REFERENCES

[1] D. Gielen, F. Boshell, D. Saygin, M. D. Bazilian, N. Wagner, and R. Gorini, "The role of renewable energy in the global energy transformation," *Energy Strateg. Rev.*, vol. 24, pp. 38–50, 2019, doi: https://doi.org/10.1016/j.esr.2019.01.006.

[2] A. Kalair, N. Abas, and N. Khan, "Comparative study of HVAC and HVDC transmission systems," *Renew. Sustain. Energy Rev.*, vol. 59, pp. 1653–1675, 2016, doi: https://doi.org/10.1016/j.rser.2015.12.288.

[3] M. J. Pérez-Molina, D. M. Larruskain, P. E. López, and G. Buigues, "Challenges for protection of future HVDC grids," *Front. Energy Res.*, vol. 8, pp. 33, 2020, doi: 10.3389/fenrg.2020.00033.

[4] S. Debnath and M. Chinthavali, "Control of MMC-HVDC in low-inertia weak grids," in *Proc. IEEE 12th Int. Conf. Power Electron. Drive Syst. (PEDS)*, Dec. 2017, pp. 435–441, doi: 10.1109/PEDS.2017.8289279.

[5] A. Mokhberdoran, A. Carvalho, N. Silva, H. Leite, and A. Carrapatoso, "Application study of superconducting fault current limiters in meshed HVDC grids protected by fast protection relays," *Electr. Power Syst. Res.*, vol. 143, pp. 292–302, 2017, doi: https://doi.org/10.1016/j.epsr.2016.09.008.

[6] C. W. K. Schwartz Justin, S. Federico, and R. Samuel, "United states patent application publication schwartz," U.S. 20170179364, 2017.

[7] G. Alvarez-Botero, F. E. Baron, C. C. Cano, O. Sosa, and M. Varon, "Optical sensing using fiber bragg gratings: Fundamentals and applications," *IEEE Instrum. Meas. Mag.*, vol. 20, no. 2, pp. 33–38, Apr. 2017, doi: 10.1109/MIM.2017.7919131.

[8] A. A. Yang Zhisheng, "Hotspot monitoring for superconducting device," PCT/IB2019/057271, 2020.

[9] P. Tixador *et al.*, "Status of the european union project FASTGRID," *IEEE Trans. Appl. Supercond.*, vol. 29, no. 5, 2019, Art. no. 5603305.

[10] A. Akbar, Z. Yang, S. Wang, L. Thévenaz, and B. Dutoit, "Optical fibre sensing for fast hotspot detection in SFCLs," *Supercond. Sci. Technol.*, vol. 33, no. 11, pp. 115003, Sep. 2020, doi: 10.1088/1361-6668/abb200.

[11] A. D. Kersey *et al.*, "Fiber grating sensors," *J. Light. Technol.*, vol. 15, no. 8, pp. 1442–1462, 1997, doi: 10.1109/50.618377.

[12] COMSOL Multiphysics v. 5.4, [Online]. Available: https://www.comsol.ch/, Accessed on: Oct. 22, 2020.

[13] N. Bagrets, S. Otten, K. P. Weiss, A. Kario, and W. Goldacker, "Thermal and mechanical properties of advanced impregnation materials for HTS cables and coils," *IOP Conf. Ser. Mater. Sci. Eng.*, vol. 102, no. 1, 2015, doi: 10.1088/1757-899X/102/1/012021.

[14] National Institute of Standards and Technology, "Material properties: Polyimide (Kapton)," [Online]. Available: https://trc.nist.gov/cryogenics/materials/Polyimide Kapton/PolyimideKapton_rev.htm, Accessed on: Oct. 22, 2020

[15] S. Zou, V. M. R. Zermeño, and F. Grilli, "Simulation of stacks of high-temperature superconducting coated conductors magnetized by pulsed field magnetization using controlled magnetic density distribution coils," *IEEE Trans. Appl. Supercond.*, vol. 26, no. 3, Apr. 2016, Art. no. 8200705.

[16] National Institute of Standards and Technology, "Material properties: Copper," [Online]. Available: https://trc.nist.gov/cryogenics/materials/OFHC Copper/OFHC_Copper_rev1.htm, Accessed on: Oct. 22, 2020.

[17] F. Roy, "Modeling and characterization of coated conductors applied to the design of superconducting fault current limiters," pp. 98, 2010, doi: 10.5075/epfl-thesis-4721.